ACS Catalysis

Research Article

pubs.acs.org/acscatalysis

Role and Evolution of Nanoparticle Structure and Chemical State during the Oxidation of NO over Size- and Shape-Controlled Pt/γ-Al_2O_3 Catalysts under Operando Conditions

E. Lira,[†] L. R. Merte,[†] F. Behafarid,[†] L. K. Ono,[†] L. Zhang,[‡] and B. Roldan Cuenya*[,§]

[†]Department of Physics, University of Central Florida, Orlando, Florida 32816, United States

[‡]Center for Functional Nanomaterials, Brookhaven National Laboratory, Upton, New York 11973, United States

[§]Department of Physics, Ruhr University Bochum, 44780 Bochum, Germany

Supporting Information

ABSTRACT: The structure and chemical state of size-selected Pt nanoparticles (NPs) supported on γ-Al_2O_3 were studied during the oxidation of NO using X-ray absorption near-edge spectroscopy and extended X-ray absorption fine-structure spectroscopy measurements under operando conditions. The data revealed the formation of PtO_x species in the course of the reaction that remained present at the maximum temperature studied, 350 °C. The PtO_x species were found in all samples, but those with the smallest NPs showed the highest degree of oxidation. Moreover, NO-induced nanoparticle redispersion was observed at temperatures below 150 °C for all catalysts studied. Catalytic tests showed activity toward the oxidation of NO for all samples. Nevertheless, the catalyst with the smallest NPs was found to be the least active, which is explained by a more extensive formation of PtO_x species in this catalyst and their detrimental contribution to the oxidation of NO.

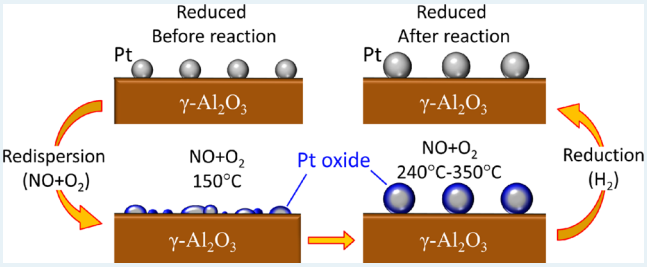

KEYWORDS: *NO oxidation, Pt nanoparticle, Al_2O_3, nanoparticle redispersion, PtO_x, EXAFS, XANES, TEM, mass spectroscopy*

1. INTRODUCTION

Stronger environmental regulations implemented in recent years have spurred interest in optimizing catalytic processes that decrease the amount of NO_x released from car engines.[1] Lean burn gasoline and diesel vehicles have become popular for their better fuel economy. However, because excess O_2 is used in these vehicles, the rate of NO_x reduction over traditional three-way catalysts is reduced. This problem is currently being addressed through the development of more efficient NO_x storage and reduction (NSR) processes.[2−4] These processes use catalysts with dual functionality: a storage function, typically utilizing a Ba-oxide-based material; and an oxidation−reduction function, typically based on Pt.[1−3] During lean operation conditions (i.e., in an oxidizing gas mixture), the NO is oxidized to NO_2 and subsequently stored in the Ba component. During fuel-rich conditions (i.e., in a reducing gas mixture), the NO_2 is reduced to N_2 and released to the atmosphere. In the present work, we focus on the properties of Pt catalysts under lean operation conditions during the oxidation of NO to NO_2, a critical step in the NSR process.

Numerous research groups have performed experimental studies of NO oxidation over Pt-based catalysts,[5−14] global rate equations have been calculated, and microkinetic models have been reported.[2,6,8,13,15−20] In some of these studies, the formation of platinum oxide (PtO_x) species or the presence of chemisorbed oxygen have been discussed to play an important role in catalyst deactivation during the oxidation of NO. For example, the reaction rate per metal surface site was found to be dependent on the Pt nanoparticle (NP) size, with larger NPs showing higher activity.[5,7] This was explained by the greater ease with which PtO_x species are formed on small Pt NPs, since such species are generally considered to be less active for the oxidation of NO than metallic Pt.[5,7,14] Along these lines, deactivation of the Pt catalysts in the course of the reaction has also been suggested to correlate with the onset of platinum oxide formation.[10] Furthermore, oxidative pretreatments with O_2 or NO_2 were found to reduce the activity of Pt catalysts toward the oxidation of NO.[5,15]

More recently, it has been shown that the oxidation of NO follows a reverse hysteresis upon temperature cycling, which means that higher catalytic activities are detected with increasing temperature, as compared with the reverse loop.[16,17] This effect was explained by the reversible reduction−oxidation of Pt. It was considered that at low temperature, NO reduces the Pt surface, and at high temperature O_2 and the NO_2 present in the gas stream contribute to its oxidation. Because PtO_x species are thought to be less reactive for the oxidation of NO, lower activities are to

Received: January 31, 2014
Revised: April 25, 2014
Published: April 25, 2014

   dx.doi.org/10.1021/cs500137r | ACS Catal. 2014, 4, 1875−1884

Table 1. Description of Synthesis Parameters and TEM Diameter of the Pt/γ-Al_2O_3 Catalysts[a]

			TEM diameter (nm)				
sample	polymer	L	as prepared	after reaction at 350 °C	after reaction at 470 °C	chemisorption Pt surface area (m^2/g-cat) as prepared	XPS Al-2p/Pt-4d area ratio normalized by as prepared Pt1
Pt1	PS(16000)-P2VP(3500)	0.05	0.6 ± 0.2	0.8 ± 0.3	0.7 ± 0.3	2.7	1
Pt2	PS(27700)-P2VP(4300)	0.06	0.6 ± 0.2	0.9 ± 0.4	0.8 ± 0.3		1.04
Pt3	PS(27700)-P2VP(4300)	0.2	0.5 ± 0.2	0.8 ± 0.3	0.7 ± 0.3	2.0	0.72

[a]The parameter "L" represents the metal salt-to-polymer head (P2VP) molecular ratio used in the NP synthesis

be expected in the reverse temperature loop (i.e., with decreasing temperature), since the initial state of the catalyst under those conditions would be oxidized. These conclusions were drawn based on catalytic tests and modeling. Nevertheless, discrepancies can be found in the literature regarding the chemical state of the Pt species at different stages of this reaction, with some groups reporting the presence of chemisorbed O on Pt,[11] while others describe the formation of PtO_x.[5,7,8,14]

Only a few groups have successfully monitored the evolution of the chemical state of the active catalysts for the oxidation of NO under reaction conditions. For instance, Pazmiño et al.[21] used operando X-ray absorption near-edge structure (XANES) and in situ extended X-ray absorption fine-structure (EXAFS) spectroscopy (room temperature measurements after reaction) to investigate such an effect, in addition to the role of sulfur and the long-term catalyst aging. Pt/SBA-15 catalysts with average NP sizes of 2.3, 3.8, and 9.0 nm were studied, and it was found that after exposing the catalysts to reaction conditions (250 °C, 300 ppm of NO, 170 ppm of NO_2, 10% O_2, balance He), the catalyst containing the smallest NPs was completely oxidized within 6 min, whereas the other two remained only partially oxidized even after 18 h of exposure. From this observation, it was concluded that only surface oxidation took place, and that such oxidation was responsible for the deactivation of the catalyst during the oxidation of NO. Boubnov et al. also used operando XANES and in situ EXAFS to study the size effects in Al_2O_3-supported Pt catalysts (1.2 to 10 nm in size) for the oxidization of NO.[22] A correlation among catalytic activity, oxidation state, and particle size was also reported, with higher turnover frequencies (TOFs) for the catalyst with the largest Pt NPs.

Although the previous studies provide important insight on structure/chemical state/reactivity correlations during the oxidation of NO, key information regarding possible morphological transformations of the catalysts in the course of the reaction is still missing. For instance, operando XANES measurements such as the ones reported above provide valuable information regarding the evolution of the chemical state of the Pt, but they cannot be used to differentiate whether the oxygen detected is present as part of an oxide structure or in its chemisorbed state.

In this study, operando EXAFS characterization at various stages of the reaction was used to determine the nature of the Pt−O bonds observed, allowing us to separate the NP-support interfacial Pt−O species from Pt oxides based on their distinct bond length, and PtOx species from chemisorbed oxygen based on the concurrent decrease of the Pt−Pt contribution upon oxide formation. It will also be illustrated that such important information can be obtained only when well-defined (size-controlled) model catalysts are considered and evaluated not simply before and after reaction, but under operando conditions.

In this work, we have prepared small size-selected Pt NPs with different sizes via inverse micelle encapsulation. The activity of these catalysts for the oxidation of NO was tested, and the evolution of their structure and chemical state was monitored under reaction conditions via X-ray absorption fine-structure spectroscopy (XAFS). Several interesting effects were observed, including NO-induced redispersion of the NPs at low temperature (<150 °C) and the formation of PtO_x species at high temperature, which remained present in our samples until at least 350 °C. Finally, a size-dependent reactivity was obtained, with the smallest and most oxidized NPs being the least active (lower TOF).

2. EXPERIMENTAL SECTION

2.1. Sample Preparation. The Pt/γ-Al_2O_3 catalysts used in this study were prepared by impregnating commercial nanocrystalline γ-Al_2O_3 (Inframat Advanced Materials, surface area ~150 m^2/g) with Pt NPs synthesized via an inverse micelle encapsulation method.[23−27] Polystyrene-*b*-poly(vinylpiridine) diblock copolymers were dissolved in toluene and subsequently loaded with $H_2PtCl_6{\cdot}6H_2O$. This preparation method allows the metal NP size to be controlled by either changing the length of the polymer head (P2VP) or by varying the metal precursor/P2VP ratio. The target Pt weight percentage in our catalysts was 1%; however, it should be noted that this loading could slightly change among the different samples prepared due to the loss of small amounts of Pt during the filtering of the micellar NP solutions taking place prior to the impregnation of the Al_2O_3 support. After impregnation, polymer removal was performed by calcining the samples at 375 °C in a mix of O_2 and He (70/30) for 24 h. Three Pt NP catalysts were prepared and characterized for this study, and the details of their preparation are described in Table 1.

2.2. Morphological, Structural, Electronic, and Chemical Characterization (AFM, XPS, XANES, EXAFS). Atomic force microscopy (AFM) was used to characterize the morphology and size distribution of the NPs before impregnation on the nanocrystalline γ-Al_2O_3 support. AFM images were acquired on dip-coated SiO_2/Si(111) wafers using a Digital Instrument Nanoscope III microscope. To check the quality of the NP solution, AFM images were taken before and after polymer removal in ultrahigh vacuum by an oxygen-plasma treatment (P_{O_2} = 5 × 10^{-5} mbar, 2.5 h).

High-angle annular dark field scanning transmission electron microscopy (HAADF-STEM) images were acquired on the different samples before and after NO oxidation using a Hitachi 2700C aberration-corrected microscope. The emission gun was operated at 200 kV, and the probe size was <0.1 nm. The TEM

dx.doi.org/10.1021/cs500137r | ACS Catal. 2014, 4, 1875−1884

samples were prepared by suspending the powder catalysts in methanol and drop-coating this suspension onto carbon-coated, 300 mesh TEM Cu grids. The Pt NP diameters were determined by measuring the full width at half-maximum of the HAADF intensity profile across individual Pt NPs.

X-ray photoelectron spectroscopy (XPS) measurements were performed on the powder samples after impregnation and calcination using a monochromatic Al Kα X-ray source and a hemispherical electron energy analyzer (SPECS GmbH). The charging of the samples was compensated by using a flood gun (7.5 eV), and the Al-2p core level peak was used for binding energy calibration and intensity normalization. The XPS data were acquired ex situ on the oxidized Pt NP catalysts directly after removal of the polymeric ligands by oxygen pretreatment. No residual carbon from the polymeric NP synthesis or Cl from the metal precursor salt (Supporting Information Figure S1b) was detected via XPS after calcination. In addition, despite the sample's brief exposure to air, no significant carbon contamination was measured on our oxidized Pt NPs. This is likely due to the weak PtO_x–CO binding on the surface of our oxidized NPs. Because of a complete overlap between Al-2p and Pt-4f signals, the second strongest Pt XPS doublet—namely, Pt-4d—was measured and used for the normalization of the reactivity data. Pt-$4d_{5/2}$ photoemission peaks at ~316 eV were observed for all samples, revealing the presence of oxidized platinum species (see Figure S1a in the Supporting Information, SI).

The catalytic reactivity of the Pt/γ-Al_2O_3 catalysts toward NO oxidation was studied using a packed-bed mass flow reactor interfaced to a quadrupole mass spectrometer (Hiden Analytical Ltd.). The reactor tube was made of quartz and had an inner diameter of 7 mm. The reactant gas mixture (400 ppm of NO, 10% O_2, balanced with He) was introduced to the system using a mass flow controller (MKS). Each measurement was repeated twice with different portions of the same fresh sample to ensure the reproducibility of the results. The data shown correspond to the average of these two measurements, and the error bars are the maximum/minimum conversion obtained from the repeated experiments. For each test, 50 mg of catalyst was used. Before the reaction, the catalysts were reduced in hydrogen (20% H_2, 80% He) at 375 °C for 2 h. Each reaction was studied at different temperatures to gain insight into the possible dependence of the onset reaction temperature with metal NP structure. The maximum temperature studied was 470 °C. At each temperature, the reaction was allowed to reach steady-state conditions, and these data were used to calculate the catalytic activity shown.

EXAFS and XANES experiments were carried out at the National Synchrotron Light Source (NSLS) at Brookhaven National Laboratory (beamline X18B). The Pt catalysts were analyzed in a continuous-flow XAFS reactor cell consisting of a Kapton tube connected to the gas lines using Teflon ferrules and quartz inserts. The transparency of the Kapton to the X-rays allows the EXAFS measurements to be carried out under operando conditions. However, the use of this material limited our maximum reaction temperature to 350 °C. Absorption spectra from the Pt-L_3 edge were collected in transmission mode. A Pt foil was measured simultaneously with the sample for calibration purposes. The samples were measured as prepared (i.e., after calcination), after reduction in hydrogen, and under reaction conditions at 25 (RT), 150, 240, and 350 °C. Multiple spectra were acquired under each experimental condition and averaged to improve the signal-to-noise ratio. The data were processed and analyzed using the Athena and Artemis software from the IFEFFIT package.[28,29] The Athena software was used for background subtraction and alignment of the spectra with the simultaneously acquired Pt foil. Following the alignment, the smooth isolated atom background was removed using the Autobk algorithm. The resultant k^2-weighted $\chi(k)$ function was fit in r space using the Artemis software package. Theoretical EXAFS signals were constructed using the FEFF8 program[30] and the model structure of bulk face centered cubic Pt. Typical k ranges used in the analysis were 2.5–13 $Å^{-1}$, and r ranges were 1.2–3.1 $Å^{-1}$. These fit ranges were adjusted depending on the temperature. The structural parameters obtained from the EXAFS fits as well as details on the fit quality for Pt1, Pt2, and Pt3 are summarized in Tables S1, S2, and S3 of the Supporting Information.

The chemisorption data were acquired for samples Pt1 and Pt3 (Micrometics, ASAP 2020). For sample Pt2, the chemisorption data is not provided because a smaller amount of material was available after the different sample characterization procedures, which led to a lack of measurement reliability for that particular sample.

3. RESULTS AND DISCUSSION

3.1. Morphology. Figure 1 displays a representative AFM image of the NPs in sample Pt3 after ligand removal, showing good size selection. The average AFM NP height in this sample was 1.5 ± 0.4 nm.

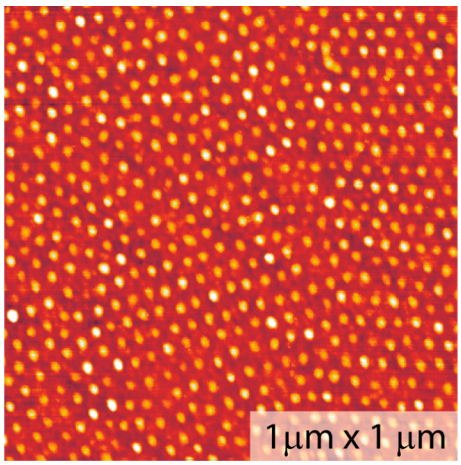

Figure 1. AFM image of Pt NPs supported on SiO_2 (4 nm)/Si(111) acquired after ligand removal via an O_2-plasma treatment in ultrahigh vacuum. The image corresponds to the same NP solution used for the synthesis of Pt3.

Figure 2 shows HAADF-STEM images from sample Pt1 after the following treatments: (a) annealing in O_2 at 375 °C (as prepared sample), (c) after NO oxidation at 350 °C (max. reaction temperature for the operando XAFS work), and (e) after NO oxidation at 470 °C (the maximum temperature for the catalytic activity test). The respective NP diameter histograms are shown in Figure 2(b,d,f).

Similar data for Pt2 and Pt3 can be found in the SI (Figures S2 and S3). The STEM data show slightly larger average NP diameters after reaction at 350 °C, indicating moderate NP sintering; however, increasing the reaction temperature to 470 °C did not seem to cause further sintering. All of the samples prepared showed very similar average TEM diameters after

dx.doi.org/10.1021/cs500137r | ACS Catal. 2014, 4, 1875–1884

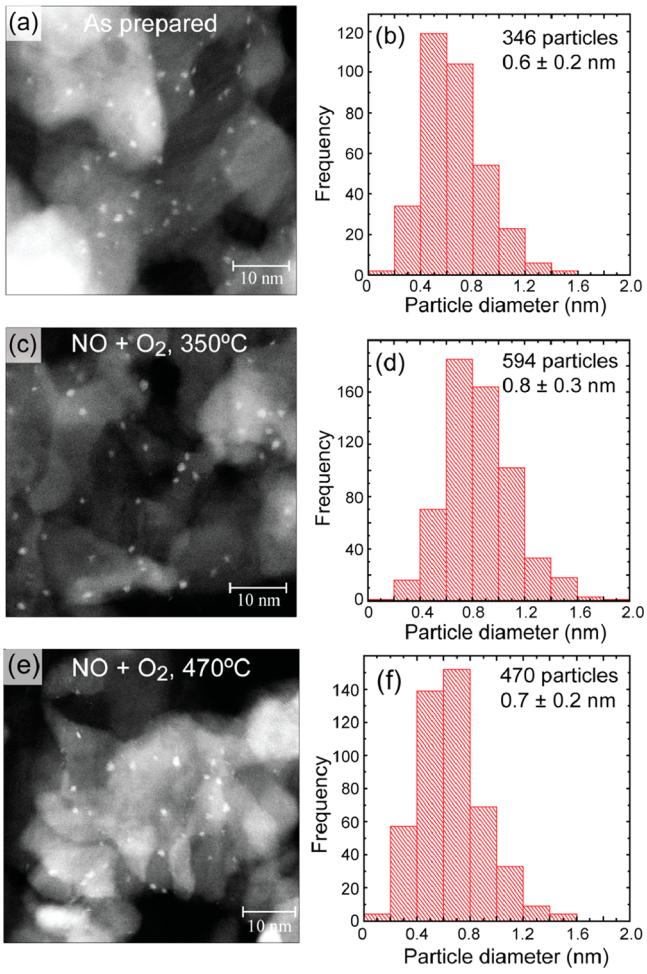

Figure 2. HAADF STEM images of Pt NPs on γ-Al_2O_3 in Pt1 and the corresponding NP diameter histograms obtained after the following treatments: (a,b) calcination in O_2 at 375 °C for 24 h (as-prepared sample), (c,d) NO + O_2 reaction at 350 °C, and (e,f) NO + O_2 reaction at 470 °C.

being exposed to the same treatments, with average sizes remaining below 1 nm after reaction at 470 °C. TEM diameters obtained for Pt1−Pt3 after different treatments are shown in Table 1.

3.2. Catalytic Activity. The catalytic performance of the different samples during the oxidation of NO is illustrated in Figure 3 as a function of the reaction temperature. All samples were reduced in situ in H_2 at 375 °C before the reactivity

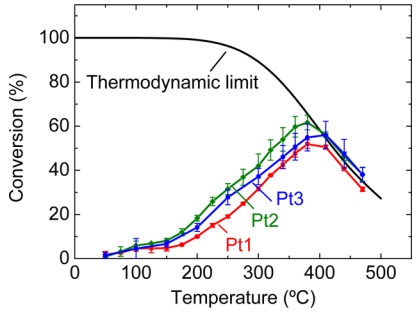

Figure 3. NO conversion during the catalytic oxidation of NO with O_2 using Al_2O_3-supported nanosized Pt catalysts. The solid line shows the expected trend following thermodynamic equilibrium.

measurements. All catalysts showed an increase in conversion with temperature, with a maximum appearing at ∼380 °C. At higher temperatures, the conversion declined, as expected from the thermodynamic equilibrium of this reaction, NO + O_2 ↔ NO_2 (solid line). The normalized conversions (TOF and XPS normalized data) are shown and discussed later in the "size and shape effect" section.

3.3. Adsorbate Chemisorption and Evolution of the NP Structure. XANES spectra from the Pt L_3-edge provide information on the unoccupied electron density of d states. Figure 4a displays Pt L_3-edge XANES spectra of Pt1 acquired at

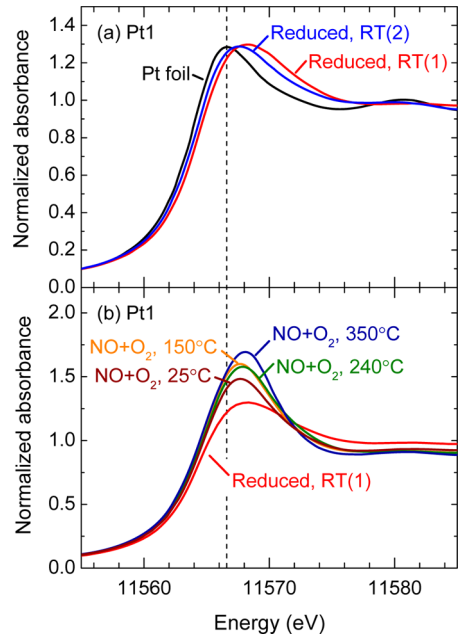

Figure 4. Pt L_3-edge XANES spectra of Pt NP/γ-Al_2O_3 NPs in Pt1. (a) Reduced NPs measured in H_2 at 25 °C before [RT(1)] and after [RT(2)] reaction. The spectrum of a Pt foil is also shown for reference. (b) Pt L_3-edge XANES spectra acquired under operando conditions during the oxidation of NO at 25, 150, 240, and 350 °C. The vertical dashed line indicates the position for the Pt foil.

25 °C after reduction in H_2 at 240 °C before [RT(1)] and after reaction [RT(2)]. Figure 4b shows XANES data acquired under reaction conditions in NO + O_2 at 25, 150, 240, and 350 °C. For reference, the spectrum obtained for the Pt foil is also shown in Figure 4a. Analogous results for Pt2 and Pt3 are shown in Figure S4 (SI). After the reduction treatment in H_2, the spectra obtained for all samples resemble that of the Pt foil, indicating the presence of metallic platinum. However, the XANES absorption peaks (white line, WL) for all reduced samples measured in H_2 are broader and shifted to higher energies with respect to the bulk Pt reference, which is mainly due to the chemisorption of hydrogen.[31−35] Figure 4a shows that the WL of the re-reduced sample measured after the NO oxidation reaction (up to 350 °C) is narrower and shifted to lower energy as compared to that of the same sample before the reaction. This observation is indicative of growth in the average NP size over the course of the reaction, since larger NPs will have a smaller fraction of lower-coordinated surface atoms available for hydrogen chemisorption. This result is consistent with the slight increase in the average NP diameter extracted from the STEM measurements in Figure 2. The same trend was observed for Pt2 (SI Figure S4a), whereas only a slight change

dx.doi.org/10.1021/cs500137r | ACS Catal. 2014, 4, 1875−1884

in the peak position and width were observed for Pt3 (SI Figure S4c). It should be kept in mind that NPs with different shapes would also have a different number of surface atoms available for chemisorption,[32] which would also influence the extent of the energy shift and peak broadening observed.

After exposing Pt1 to NO and O_2 at 25 °C (Figure 4b), the position of the WL peak shifted back to lower energy, while an increase in the intensity (WL height) was observed. Such a change is indicative of an increase in the density of unoccupied d electronic states and, thus, an increase in Pt oxidation state due to the presence of chemisorbed oxygen on the NP surface or to the formation of Pt oxide under the oxidizing reaction environment.[36] It will be shown in the next section that, in fact, such an increase is due to the formation of PtO_x.

Pt-L_3 edge EXAFS spectra were also measured for all samples in hydrogen before and after reaction and under NO oxidation conditions at 25 (RT), 150, 240, and 350 °C. Figure 5a shows

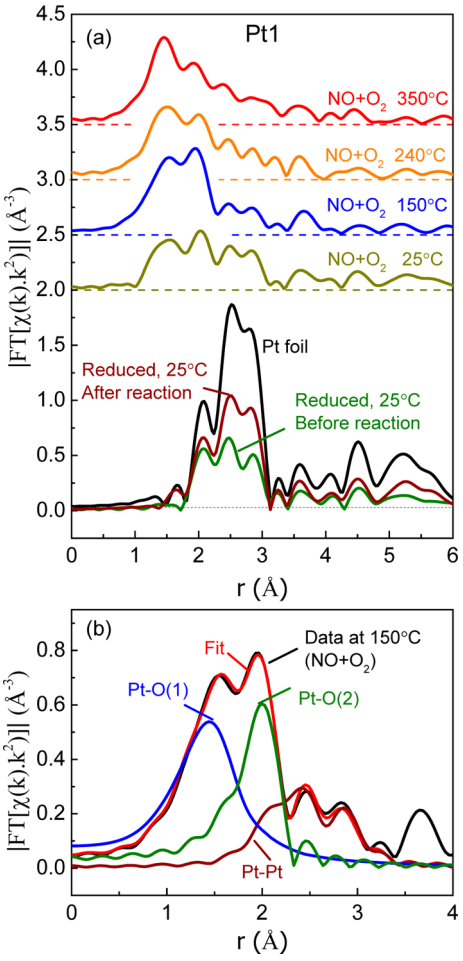

Figure 5. (a) k^2-weighted Fourier transformed Pt-L_3 edge EXAFS spectra (r space) of Pt NPs/γ-Al_2O_3 in Pt1, acquired in the following environments and after different pretreatments: reduced NPs measured in H_2 at 25 °C before and after reaction, and spectra acquired under operando conditions during the oxidation of NO at 25, 150, 240, and 350 °C. The spectrum of a Pt foil is also shown for reference. (b) Representative Fourier transformed Pt-L_3 edge EXAFS spectrum of sample Pt1 acquired during the oxidation of NO at 150 °C together with the corresponding fit using metallic Pt−Pt, Pt−O(1), and Pt−O(2) scattering paths. For each sample, the NPs were measured in their reduced state at 25 °C before and after reaction. The k range used for the Fourier transformation is 2.5−13 $Å^{-1}$.

the k^2-weighted Fourier-transform spectra from Pt1, and those from Pt2 and Pt3 are shown in Figure S5 (SI). For comparison, reference data for a Pt foil acquired at 25 °C are also shown. An overall damping of the spectra was observed for all NP samples as compared with bulk Pt, which indicates reduced atomic coordination numbers and enhanced structural disorder in the NP samples, resulting from the small size of the particles.

Figure 5b shows EXAFS data acquired for Pt1 during the oxidation of NO at 150 °C together with a representative fit, for which three components were used: (i) metallic Pt−Pt (~2.75 Å), Pt−O(1) (~2.0 Å), and Pt−O(2) (~2.5 Å). All bond length values given here are phase-corrected. Details on the fitting procedure, fit parameters, and additional example fits can be found in the SI (Figures S6−S8, Tables S1−S3). In agreement with previous literature, the Pt−O(1) contribution at ~2 Å is assigned to PtO_x species.[37,38] To our knowledge, a Pt−O(2) contribution has not been reported either for bulk PtO or PtO_2, or for oxides formed on extended single crystal surfaces. On the basis of previous reports, we tentatively assign this contribution to scattering paths at the NP−support interface.[39−44] A similar long Pt−O(2) bond has been previously observed experimentally for Pt NPs supported on zeolites and γ-Al_2O_3 when the samples were reduced at low temperature (<350 °C) or when the support was hydroxylated, and it was assigned to Pt−O−H scattering paths at the NP-support interface.[40,44−48] More recently, theoretical calculations for small Pt NPs on hydroxylated γ-Al_2O_3 also showed the possibility of a ~2.5 Å bond distance due to Pt−O−H or Pt−Al bonds, in either case reflecting the interaction between the Pt NP and the alumina support.[41,49]

Such long Pt−O bonds have also been found for Pt/γ-Al_2O_3 samples prepared with $(NH_3)_4Pt(OH)_2$ precursors, ruling out a Pt−Cl scattering path due to chlorine contamination as the origin of this component.[44] This is especially true in our study in which the XPS data did not show any detectable Cl-2p signal (SI Figure S1b). In addition, as will be shown later, the long Pt−O contribution increases at temperatures below 150 °C. This is another evidence for ruling out a possible Pt−Cl contribution, since the content of Cl (and Pt−Cl bonds) in our samples should not increase with temperature, especially given that our samples were preannealed for 24 h in O_2 at much higher temperature (375 °C).

In addition, it is worth mentioning that the features fitted in our EXAFS analysis by a long Pt−O bond could not be considered as a short Pt−Pt bond. Because of the large difference between the atomic numbers of O (8) and Pt (78), the scattering behavior of these two elements are starkly different in their intensity, phase shift, and features. The multiple-peak shape of a Pt−Pt bond cannot appear at such low R values, even in the case of an exaggerated bond contraction, and would not be able to reproduce the narrow and sharp peak at ~2 Å.

Figure 6 displays the evolution of the first nearest neighbor (NN) coordination numbers (CNs) of samples (a) Pt1, (b) Pt2, and (c) Pt3 during the oxidation of NO extracted from the analysis of the EXAFS data in Figure 5 and SI Figure S5. After the initial reduction in H_2 at 240 °C, all samples showed a dominant Pt−Pt contribution and a small Pt−O(2) contribution (Figure 6). The Pt−Pt CN for Pt1 was the smallest, and that of Pt3, the largest. However, when the catalysts were reduced after the reaction and measured under H_2, the intensity of the Pt−Pt EXAFS components and the respective coordination numbers showed an increase with respect to

dx.doi.org/10.1021/cs500137r | ACS Catal. 2014, 4, 1875−1884

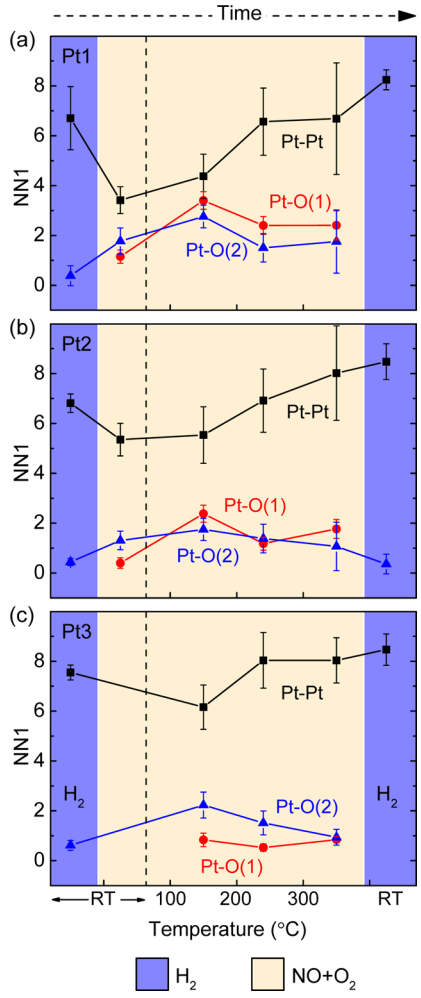

Figure 6. Evolution of the first-nearest-neighbor (NN1) coordination numbers extracted from the fits of EXAFS data acquired for Pt NPs/γ-Al_2O_3 in (a) Pt1, (b) Pt2, and (c) Pt3 before, during, and after the oxidation of NO. Three curves corresponding to Pt−Pt (~2.75 Å, squares), Pt−O(1) (~2.0 Å, circles), and Pt−O(2) (~2.5 Å, triangles) contributions are shown. The blue area indicates data acquired at 25 °C after reduction in H_2 before and after the reaction, and the yellow-shaded area indicates data acquired during the oxidation of NO.

those of the catalysts in their initial state before reaction. Such a slight increase in the NP size after the reaction is in agreement with the changes in the XANES data discussed in the previous section as well as with the direct observation through STEM measurements. Because all of these catalysts were preannealed in O_2 at 375 °C before the reaction for 24 h, the morphological change observed after reaction at 350 °C cannot be assigned to thermally induced NP sintering that can occur in O_2, but rather, to a change driven by the presence of NO and the oxidation reaction itself.

Figure 6a reveals that the exposure of Pt1 to NO and O_2 at 25 °C resulted in a decrease in the main metallic Pt−Pt peak, the appearance of a Pt−O(1) contribution, and a drastic increase of the long Pt−O component [Pt−O(2)]. The Pt−O(1) component represents both, PtO_x species and chemisorbed oxygen on the Pt NP surface. However, the appearance of such component concomitant with the decrease in the Pt−Pt CN indicates the formation of PtO_x species. On the other hand, because the Pt−O(2) component is associated with the NP-support interface, changes in this component should be related to the extent of the Pt-support contact area. The increase observed in the Pt−O(2) component from room temperature up to 150 °C could have two origins: (i) the flattening of oxidized NPs, or (ii) NP fragmentation and redispersion because both result in a larger NP/support interfacial area. In recent studies by our group, a similar feature due to long metal−oxygen bonds (2.5−2.6 A) was also detected for Pd NPs before the onset of the selective reduction of NO with H_2,[42] and for Pt NPs during the oxidation of isopropanol.[50]

In the case of NO reduction, an increase in the long Pd−O bond component with increasing temperature was observed. Because of the absence of oxygen in that case, this phenomenon was unambiguously assigned to NO-induced NP redispersion, leading to the formation of small clusters. Similarly, the redispersion explanation is the most plausible in this study, considering both the strong binding of NO to Pt, and also the fact that the chemical state of the NPs does not change significantly with increasing temperature from 25 to 150 °C once the NPs have already been exposed to the reactants.

3.4. Oxidation State Effects. All the scattering components [i.e., Pt−Pt, Pt−O(1) and Pt−O(2)] were consistently present under the NO + O_2 environment as the temperature was further increased to 150, 240, and 350 °C. Therefore, in the course of the reaction, the Pt NPs were partially oxidized. Because XAFS provides information on the entire sample, contribution from metallic or partially oxidized large grains of Pt cannot be ruled out; however, it should be mentioned that such large grains were not observed in these samples by TEM.

Different oxide structures have been shown to exist on extended platinum (110) surfaces during CO oxidation, depending on the specific reaction conditions, including the pressure and the ratio of O_2/CO. Such different oxide structures were found to affect the catalytic activity of the NPs,[51−53] but regardless of the oxide structure, there are some indications in the current literature that platinum oxide species increase the CO oxidation activity.[52,53] However, the effect of Pt oxide species in the reaction rate may vary for different reactions. For instance, in clear contrast with the CO oxidation process, the presence of oxide species appears to hinder the catalyst activity in NO oxidation reactions.[5,7,14]

Using microkinetic modeling, Bhatia et al.[15] proposed that the catalyst surface is predominantly covered by NO at temperatures below 150 °C in the NO oxidation reaction. Although our measurements indicate the formation of PtO_x species at low temperature under reaction conditions for our small Pt NPs (<1 nm), the possible redispersion of Pt observed up to 150 °C appears nevertheless to be caused by the strong influence of NO.[42,50,54,55]

Previous reports on the catalytic oxidation of NO indicate a strong influence of NO adsorbed at low temperature on the partial reduction of Pt. For example, Hauptman et al.[17] observed an inverse hysteresis in the conversion of NO when the temperature was linearly increased from 80 to 370 °C and subsequently decreased at a rate of 5 °C/min. The authors explained their results on the basis of the oxidation of the Pt NPs at high temperature during the initial temperature ramp, leading to decreased reactivity, followed by partial reduction by NO to metallic Pt at low temperature. Their simulations showed that PtO_x formation does not start until 150 °C in the initial heat-up cycle, and the oxide does not decompose completely at that temperature during the cool down cycle (~20% oxide coverage at 150 °C). Similar observations were made by Hauff et al.,[16] who also showed that if the temperature

dx.doi.org/10.1021/cs500137r | ACS Catal. 2014, 4, 1875−1884

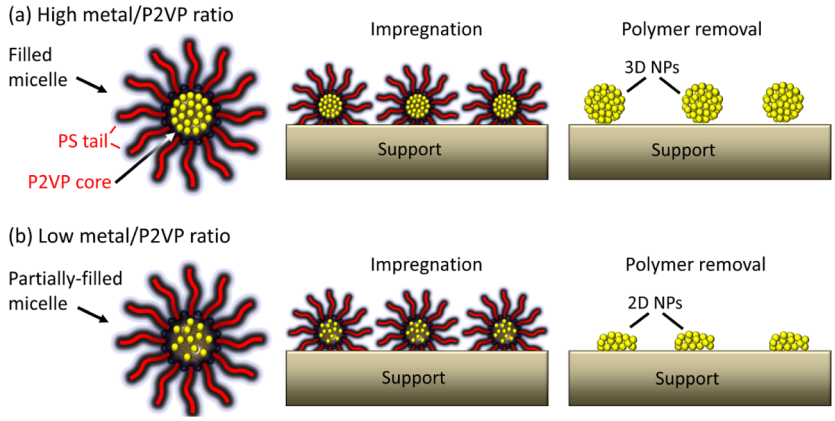

Figure 7. Schematic model of the effect of micelle metal loading, with higher loading resulting in 3D NP shapes and low loading leading to flat 2D-like NPs.

was cycled between 250 and 350 °C, the hysteresis disappeared, meaning that no catalyst reactivation through reduction by NO took place above 250 °C. In addition, it was shown that staying at each temperature for a longer time would reduce the hysteresis,[17] pointing out that if enough time is provided, the oxidation state of the catalysts would reach an equilibrium state between those during the heat-up and cool-down cycles. In the present study, each temperature was kept constant for EXAFS measurements for at least 1 h, and therefore, at 150 °C, a moderate oxide coverage is expected, in agreement with our EXAFS analysis results (Figure 6 and SI Tables S1–S3).

Furthermore, when Pt1 was exposed to NO and O_2, the presence of either chemisorbed oxygen or PtO_x species on the NP surface was evident from our XANES data (Figure 4b) because a clear increase in the intensity of the Pt-L_3 absorption peak was observed.[56] This observation is supported by the EXAFS spectra presented in Figure 5a and corresponding analysis in Figure 6a, which reveal the presence of a Pt–O scattering path with a bond distance of ~2.0 Å [Pt–O(1)]. As was mentioned before, because the appearance of the Pt–O(1) component occurred concomitantly with a decrease in the Pt–Pt component, the Pt–O(1) scattering path is assigned to the formation of PtO_x species rather than the presence of only chemisorbed oxygen. Nevertheless, the decrease in the Pt–Pt CN can also be at least partially assigned to a NO-induced NP redispersion or flattening phenomenon.

3.5. Size and Shape Effects. Although our STEM images indicated no drastic differences in the average NP size (~0.6 nm) among the different as-prepared samples, clearly distinct first NN CNs values (SI Tables S1, S2 and S3) were obtained for Pt1 and Pt2 (NN1 of 6.7 and 6.8, respectively), as compared with Pt3 (7.9). This finding can be explained by considering that the EXAFS CNs reflect not only the NP size but also their shape (a larger NN1 is observed for 3D NPs as compared with 2D NPs of the same TEM diameter).[26] Therefore, the term "size" throughout this manuscript does not refer to the NP diameters extracted by TEM, but rather is based on the overall volume of the NPs, that is, on the number of atoms in the NPs. Following this definition, Pt1 has the smallest NPs and Pt3 has the largest.

To understand the origin of the different shapes obtained for Pt1–Pt3, we need to take into account the synthesis procedure, in which lower Pt/P2VP loadings (0.05–0.06), such as that used to prepare Pt1 and Pt2, would result in flatter NPs (and lower NN1 values) as compared with those in Pt3, in which the Pt/P2VP loading was larger (0.2).[26,57] Figure 7 shows the schematic of how different micellar loadings affect the final shape of NPs after polymer removal by annealing in oxygen (375 °C).

To further compare the intrinsic catalytic activity of the different samples, a normalization procedure is required. For samples Pt1 and Pt3, the TOFs were calculated using Pt surface areas determined by CO chemisorption (Figure 8a). For such a calculation, it is required that the concentrations of the reactants does not change significantly through the catalyst bed to ensure that different portions of the catalyst experience similar reaction conditions. To achieve this, the TOFs were

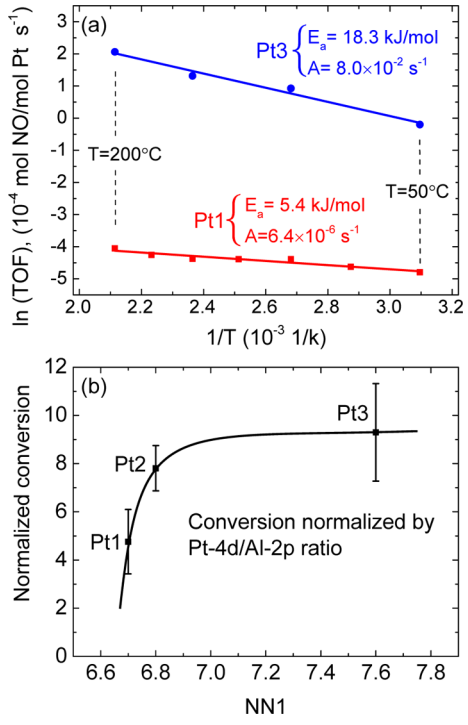

Figure 8. (a) Arrhenius plot of TOF obtained for Pt1 and Pt3 expressed as moles of NO converted per mole of surface Pt per second. The apparent activation energy and the prefactor obtained from the Arrhenius plot are also shown. (b) NO conversion obtained at 150 °C normalized by the XPS data (Pt-4d/Al-2p area ratio) of sample Pt1 versus the first-nearest coordination number (NN1) extracted from EXAFS measurements.

dx.doi.org/10.1021/cs500137r | ACS Catal. 2014, 4, 1875–1884

obtained only at low temperature, when the conversion was below 20%. Here, the TOF is defined as moles of NO converted per mole of surface Pt per second. The results are shown in Figure 8a, and they reveal that surface Pt atoms in Pt3 are much more catalytically active than those in Pt1 toward the oxidation of NO.

In addition, following a different approach, the XPS data were used to normalize the conversion data. Because the alumina support is identical in all samples and is very stable within the temperature range employed, the Pt-4d/Al-2p ratio provides a good quantitative estimation of Pt loading. Because the average size of the NPs in this study is around 0.6−0.7 nm and the inelastic mean free path of the photoelectrons at the energy of interest (~1414 eV) is about 1.7 nm, the signal attenuation is negligible. In addition, even if such attenuation is considered, it should be very similar for all of our samples having similar sizes. The same reasoning is true for the shape effect, which is even more insignificant for our samples. In this case, the ratio of integrated areas of the Pt-4d (NPs) and Al-2p (support) XPS peaks were used as a measure of the Pt content in each sample to normalize the conversion data obtained at a certain temperature (e.g., 150 °C). The Pt-4d/Al-2p ratios normalized by that of Pt1 are shown in Table 1. The results are shown in Figure 8b as a function of the first-nearest-neighbor (NN1) coordination number (CN) obtained from the analysis of EXAFS data acquired at 25 °C in H_2 on the reduced NPs before reactant exposure.

After normalizing the conversion data, a trend can be observed, with the highest activity per Pt atom found for the sample containing NPs with the largest first NN coordination number (Pt3). This could be understood a priori as an indication that larger NPs are more active for this reaction, as has been previously discussed.[5,7,14]

In addition, the XANES and EXAFS data show that sample Pt3 is more resistant to oxidation in the course of the reaction [SI Figure S4d and Figure 6; see CNs for Pt−O(1) bond] as compared with Pt1 and Pt2. This is in line with a previous study in which we have shown the more facile oxidation of flat (2D-like) NPs as compared with 3D NPs of identical average TEM diameter.[57] Therefore, the lower reactivity (TOF) observed for the flat NPs in Pt1 and Pt2 might be assigned to the more facile formation of PtO_x species in these samples. This is in agreement with previous reports addressing the effect of oxide formation during the oxidation of NO.[5,7,8,11]

To better understand the different activity (TOF) observed for Pt1 and Pt3, the activation energies were extracted from the Arrhenius plot in Figure 8a; namely, 18.3 kJ/mol for Pt3 and 5.4 kJ/mol for Pt1. These values are smaller than those reported by Schmitz et al.[58] (33−41 kJ/mol), which most likely originates from the smaller size of our NPs (<0.8 mn) as compared with theirs (~2.5 nm). Surprisingly, the sample with higher activity (TOF) shows higher activation energy (i.e., larger energy barrier), which may seem counterintuitive. However, the higher energy barrier is accompanied by a higher prefactor (4 orders of magnitude) and vice versa. This is due to the so-called compensation effect,[58−60] which has been reported for several catalytic reactions, including NO oxidation.[58] This effect is described as a linear correlation between the natural log of the prefactor and the apparent activation energies for a set of different catalysts (different metal, loading, synthesis, pretreatment, etc.). The origin of this effect has been debated for a long time and has been successfully described by Bligaard et al. on the basis of a shift in kinetic regimes.[59] Following the Brønsted−Evans−Polanyi relation, a higher adsorption enthalpy for a certain adsorbate is accompanied by a higher binding energy of the adsorbed species. Such increased binding energy would result in an excessive surface coverage (poisoning) that would prevent the other involved adsorbates from participating in the reaction. This would result in a volcano behavior for TOF as a function of adsorption enthalpy as well as a correlation between the prefactor and the activation energy. In addition, it has been shown that O_2 adsorption is the rate-limiting step in the NO oxidation reaction.[15] Therefore, our observation might be understood as a lower activation energy for O_2 dissociation in our smaller NPs (Pt1), resulting in oxygen poisoning and, consequently, a much lower prefactor. The trade-off between these two parameter results in a lower overall TOF for smaller NPs.

Furthermore, the size of the NPs was found to affect their coarsening behavior. Samples containing flatter NPs (Pt1 and Pt2) show a more substantial increase in their NN1 values after reaction, whereas Pt3, which has the most 3D character, displayed very similar NN1 numbers before and after reaction. Because of the smaller fraction of surface atoms available on Pt3 and the lower NP/support contact area, the NO-induced redispersion and subsequent reagglomeration of the small Pt clusters or ions appears not to be as significant for Pt3 as for Pt1 and Pt2.

Figure 9 schematically depicts the morphological change undergone by our NP catalysts under reaction conditions

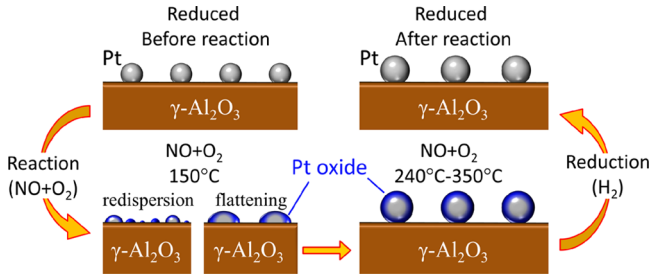

Figure 9. Schematic model of the evolution of morphology and chemical state of small Pt NPs supported on γ-Al_2O_3 during the oxidation of NO.

inferred from the analysis of STEM and operando XANES and EXAFS data. Starting with the metallic Pt NPs, exposure to NO and O_2 from 25 to 150 °C (i.e., before the onset of the NO oxidation reaction) leads to an increase in the Pt/support (hydroxylated γ-Al_2O_3) contact surface, which is caused by a change in the shape of the NPs (NP flattening), by NO-induced disaggregation and redispersion of the NPs, or by a combination of both.

Increasing the reaction temperature to 150 °C leads to the oxidation of the Pt NPs, forming PtO_x species at the NP surface. When the temperature is further increased (240 °C < T ≤ 350 °C), the particles partially dewet the surface, resulting in more rounded (3D) NP shapes but retaining PtO_x at their surface. Finally, after reducing the samples after the reaction was concluded, a slight increase in size is observed as compared with the catalyst's initial state.

Our study illustrates the dynamic changes in the structure and chemical state of nanoscale catalysts under reaction conditions, highlighting the importance of operando studies,

dx.doi.org/10.1021/cs500137r | ACS Catal. 2014, 4, 1875−1884

such as the one presented here, to gain understanding on structure−reactivity correlations.

4. CONCLUSIONS

Micellar Pt NPs supported on γ-Al_2O_3 were studied using operando XAS with the aim of gaining insight into the evolution of the structure (size and shape) and chemical state of the NPs during the oxidation of NO. Three samples with nearly identical sizes (~0.6 nm TEM) but different shapes (Pt1 and Pt2, 2D-like; Pt3, 3D-like) were synthesized, and their performances as NO oxidation catalysts were tested. The sample with the highest first-nearest-neighbor coordination number (Pt3) was the most active for the conversion of NO, which was explained by the lower degree of oxidation observed in this sample under reaction conditions. For all samples studied, NO was found to induce the redispersion or flattening of the Pt NPs at or below 150 °C, that is, before the onset of the reaction, with an associated increase in the fraction of Pt−O bonds from the NP/support interface. The formation of PtO_x species is observed at 150 °C, remaining present under reaction conditions at least until 350 °C. The Pt NPs prepared were very stable during the reaction showing that they sintered only slightly (final size ~ 0.7 nm), even after treatment at 470 °C. The results presented illustrate the usefulness of XAFS for the study of structure−reactivity relationships in complex nano-sized catalysts under operando conditions.

■ ASSOCIATED CONTENT

Supporting Information

XPS data, the TEM data and corresponding histograms (samples Pt2 and Pt3), the XANES and raw EXAFS data (samples Pt2 and Pt3), details of EXAFS analysis as well as the fitted data for all samples, and examples of *k* space and *q* space data. This material is available free of charge via the Internet at http://pubs.acs.org.

■ AUTHOR INFORMATION

Corresponding Author

*E-mail: Beatriz.Roldan@rub.de.

Notes

The authors declare no competing financial interest.

■ ACKNOWLEDGMENTS

The authors are grateful to Nebojsa Marinkovic (BNL) for beamline support and to Anatoly Frenkel (Yeshiva University) for his advice during the evaluation of the EXAFS data. This work was made possible thanks to funding from the National Science Foundation, NSF-CHE-1213182. Synchrotron Catalysis Consortium facilities at NSLS (BNL), where the XAFS measurements were conducted, are funded by the US Department of Energy (DE-FG02-05ER15688). NSLS (XAFS work) and the Center for Functional Nanomaterials (TEM work) at Brookhaven National Laboratory are supported by the U.S. Department of Energy, Office of Basic Energy Sciences, under Contract No. DE-AC02-98CH10886. This work was also supported in part by the Cluster of Excellence Ruhr Explores Solvation (RESOLV) (EXC 1069) funded by the Deutsche Forschungsgemeinschaft.

■ REFERENCES

(1) Epling, W. S.; Campbell, L. E.; Yezerets, A.; Currier, N. W.; Parks, J. E. *Catal. Rev.* **2004**, *46*, 163−245.
(2) Matsumoto, S. i. *Catal. Today* **2004**, *90*, 183−190.
(3) Rankovic, N.; Nicolle, A.; Da Costa, P. *J. Phys. Chem. C* **2010**, *114*, 7102−7111.
(4) Takahashi, N.; Shinjoh, H.; Iijima, T.; Suzuki, T.; Yamazaki, K.; Yokota, K.; Suzuki, H.; Miyoshi, N.; Matsumoto, S.-i.; Tanizawa, T.; Tanaka, T.; Tateishi, S.-s.; Kasahara, K. *Catal. Today* **1996**, *27*, 63−69.
(5) Olsson, L.; Fridell, E. *J. Catal.* **2002**, *210*, 340−353.
(6) Marques, R.; Darcy, P.; Costa, P. D.; Mellottée, H.; Trichard, J.-M.; Djéga-Mariadassou, G. *J. Mol. Catal. A: Chem.* **2004**, *221*, 127−136.
(7) Mulla, S.; Chen, N.; Cumaranatunge, L.; Blau, G.; Zemlyanov, D.; Delgass, W.; Epling, W.; Ribeiro, F. *J. Catal.* **2006**, *241*, 389−399.
(8) Mulla, S. S.; Chen, N.; Delgass, W. N.; Epling, W. S.; Ribeiro, F. H. *Catal. Lett.* **2005**, *100*, 267−270.
(9) Olsson, L.; Abul-milh, M.; Karlsson, H.; Jobson, E.; Thorma, P.; Hinz, A. *Top. Catal.* **2004**, *30/31*, 85−90.
(10) Després, J.; Elsener, M.; Koebel, M.; Kröcher, O.; Schnyder, B.; Wokaun, A. *Appl. Catal., B* **2004**, *50*, 73−82.
(11) Weiss, B. M.; Iglesia, E. *J. Phys. Chem. C* **2009**, *113*, 13331−13340.
(12) Xue, E.; Seshan, K.; Ross, J. *Appl. Catal., B* **1996**, *11*, 65−79.
(13) Olsson, L.; Persson, H.; Fridell, E.; Skoglundh, M.; Andersson, B. *J. Phys. Chem. B* **1999**, *103*, 10433−10439.
(14) Fridell, E.; Amberntsson, A.; Olsson, L.; Grant, A. W.; Skoglundh, M. *Top. Catal.* **2004**, *30/31*, 143−146.
(15) Bhatia, D.; McCabe, R. W.; Harold, M. P.; Balakotaiah, V. *J. Catal.* **2009**, *266*, 106−119.
(16) Hauff, K.; Tuttlies, U.; Eigenberger, G.; Nieken, U. *Appl. Catal., B* **2012**, *123−124*, 107−116.
(17) Hauptmann, W.; Votsmeier, M.; Gieshoff, J.; Drochner, a.; Vogel, H. *Appl. Catal., B* **2009**, *93*, 22−29.
(18) Smeltz, A. D.; Delgass, W. N.; Ribeiro, F. H. *Langmuir* **2010**, *26*, 16578−16588.
(19) Epling, W. S.; Parks, J. E.; Campbell, G. C.; Yezerets, A.; Currier, N. W.; Campbell, L. E. *Catal. Today* **2004**, *96*, 21−30.
(20) Muncrief, R. L.; Khanna, P.; Kabin, K. S.; Harold, M. P. *Catal. Today* **2004**, *98*, 393−402.
(21) Pazmiño, J. H.; Miller, J. T.; Mulla, S. S.; Nicholas Delgass, W.; Ribeiro, F. H. *J. Catal.* **2011**, *282*, 13−24.
(22) Boubnov, A.; Dahl, S.; Johnson, E.; Molina, A. P.; Simonsen, S. B.; Cano, F. M.; Helveg, S.; Lemus-Yegres, L. J.; Grunwaldt, J. D. *Appl. Catal., B* **2012**, *126*, 315−325.
(23) Ono, L. K.; Croy, J. R.; Heinrich, H.; Roldan Cuenya, B. *J. Phys. Chem. C* **2011**, *115*, 16856−16866.
(24) Ono, L. K.; Yuan, B.; Heinrich, H.; Roldan Cuenya, B. *J. Phys. Chem. C* **2010**, *114*, 22119−22133.
(25) Croy, J. R.; Mostafa, S.; Heinrich, H.; Roldan Cuenya, B. *Catal. Lett.* **2009**, *131*, 21−32.
(26) Roldan Cuenya, B.; Croy, J. R.; Mostafa, S.; Behafarid, F.; Li, L.; Zhang, Z.; Yang, J. C.; Wang, Q.; Frenkel, A. I. *J. Am. Chem. Soc.* **2010**, *132*, 8747−8756.
(27) Croy, J. R.; Mostafa, S.; Liu, J.; Sohn, Y. H.; Heinrich, H.; Roldan Cuenya, B. *Catal. Lett.* **2007**, *119*, 209−216.
(28) Newville, M. *J. Synchrotron Radiat.* **2001**, *8*, 322−324.
(29) Ravel, B.; Newville, M. *J. Synchrotron Radiat.* **2005**, *12*, 537−541.
(30) Zabinsky, S.; Rehr, J.; Ankudinov, A.; Albers, R.; Eller, M. *Phys. Rev. B* **1995**, *52*, 2995−3009.
(31) Small, M. W.; Sanchez, S. I.; Marinkovic, N. S.; Frenkel, A. I.; Nuzzo, R. G. *ACS Nano* **2012**, *6*, 5583−5595.
(32) Behafarid, F.; Ono, L. K.; Mostafa, S.; Croy, J. R.; Shafai, G.; Hong, S.; Rahman, T. S.; Bare, S.; Roldan Cuenya, B. *Phys. Chem. Chem. Phys.* **2012**, *14*, 11766−11779.
(33) Ichikuni, N.; Iwasawa, Y. *Catal. Lett.* **1993**, *20*, 87−95.
(34) Samant, M. G.; Boudart, M. *J. Phys. Chem.* **1991**, *95*, 4070−4074.
(35) Mistry, H.; Behafarid, F.; Bare, S. R.; Roldan Cuenya, B. *ChemCatChem* **2014**, *6*, 348−352.

(36) Lytle, F. W.; Wei, P. S. P.; Greegor, R. B.; Via, G. H.; Sinfelt, J. H. *J. Chem. Phys.* **1979**, *70*, 4849−4855.
(37) Lagarde, P.; Murata, T.; Vlaic, G.; Freund, E.; Dexpert, H.; Bournonville, J. P. *J. Catal.* **1983**, *84*, 333−343.
(38) Mansour, A. N.; Sayers, D. E.; Cook, J. W.; Short, D. R.; Shannon, R. D.; Katzer, J. R. *J. Phys. Chem.* **1984**, *88*, 1778−1781.
(39) Alcalá, R.; Greeley, J.; Mavrikakis, M.; Dumesic, J. A. *J. Chem. Phys.* **2002**, *116*, 8973−8980.
(40) Koningsberger, D. C.; Gates, B. C. *Catal. Lett.* **1992**, *14*, 271−277.
(41) Mager-Maury, C.; Bonnard, G.; Chizallet, C.; Sautet, P.; Raybaud, P. *ChemCatChem* **2011**, *3*, 200−207.
(42) Paredis, K.; Ono, L. K.; Behafarid, F.; Zhang, Z.; Yang, J. C.; Frenkel, A. I.; Roldan Cuenya, B. *J. Am. Chem. Soc.* **2011**, *133*, 13455−13464.
(43) Merte, L. R.; Ahmadi, M.; Behafarid, F.; Ono, L. K.; Lira, E.; Matos, J.; Li, L.; Yang, J. C.; Roldan Cuenya, B. *ACS Catal.* **2013**, *3*, 1460−1468.
(44) Koningsberger, D.; Sayers, D. *Solid State Ionics* **1985**, *16*, 23−27.
(45) Vaarkamp, M.; Miller, J. T.; Modica, F. S.; Koningsberger, D. C. *J. Catal.* **1996**, *163*, 294−305.
(46) Vaarkamp, M.; Modica, F. S.; Miller, J. T.; Koningsberger, D. C. *J. Catal.* **1993**, *144*, 611−626.
(47) Vaarkamp, M.; Grondelle, J. V.; Miller, J. T.; Sajkowski, D. J.; Modica, F. S.; Lane, G. S.; Gates, B. C.; Koningsberger, D. C. *Catal. Lett.* **1990**, *6*, 369−381.
(48) de Graaf, J.; Vandillen, A.; Dejong, K.; Koningsberger, D. *J. Catal.* **2001**, *203*, 307−321.
(49) Hu, C. H.; Chizallet, C.; Mager-Maury, C.; Corral-Valero, M.; Sautet, P.; Toulhoat, H.; Raybaud, P. *J. Catal.* **2010**, *274*, 99−110.
(50) Paredis, K.; Ono, L. K.; Mostafa, S.; Li, L.; Zhang, Z.; Yang, J. C.; Barrio, L.; Frenkel, A. I.; Roldan Cuenya, B. *J. Am. Chem. Soc.* **2011**, *133*, 6728−6735.
(51) Newton, M. A.; Chapman, K. W.; Thompsett, D.; Chupas, P. J. *J. Am. Chem. Soc.* **2012**, *134*, 5036−5039.
(52) Ackermann, M.; Pedersen, T.; Hendriksen, B.; Robach, O.; Bobaru, S.; Popa, I.; Quiros, C.; Kim, H.; Hammer, B.; Ferrer, S.; Frenken, J. *Phys. Rev. Lett.* **2005**, *95*, 255505.
(53) Hendriksen, B.; Frenken, J. *Phys. Rev. Lett.* **2002**, *89*, 046101.
(54) Ali, A.; Alvarez, W.; Loughran, C. J.; Resasco, D. E. *Appl. Catal., B* **1997**, *14*, 13−22.
(55) Che, M.; Dutel, J. F.; Gallezot, P.; Primet, M. *J. Phys. Chem.* **1976**, *80*, 2371−2381.
(56) Qi, B.; Perez, I.; Ansari, P.; Lu, F.; Croft, M. *Phys. Rev. B* **1987**, *36*, 2972−2975.
(57) Mostafa, S.; Behafarid, F.; Croy, J. R.; Ono, L. K.; Li, L.; Yang, J. C.; Frenkel, A. I.; Roldan Cuenya, B. *J. Am. Chem. Soc.* **2010**, *132*, 15714−15719.
(58) Schmitz, P.; Kudla, R.; Drews, A.; Chen, A.; Lowema, C.; McCabe, R.; Schneider, W.; Goralskijr, C. *Appl. Catal., B* **2006**, *67*, 246−256.
(59) Bligaard, T.; Honkala, K.; Logadottir, A.; Norskov, J. K.; Dahl, S.; Jacobsen, C. J. H. *J. Phys. Chem. B* **2003**, *107*, 9325−9331.
(60) Logadottir, A. *J. Catal.* **2001**, *197*, 229−231.